Pergamon

Int. J. Solids Structures Vol. 32, No. 17/18, pp. 2523–2546, 1995

0020–7683/95 $9.50 + .00

0020–7683(94)00281–9

EFFECT OF FLAWS ON THE STRESS WAVE PROPAGATION IN PARTICULATE AGGREGATES: NEAR AND FAR FIELD OBSERVATIONS

RAMAN SINGH and ARUN SHUKLA
Dynamic Photomechanics Laboratory, Department of Mechanical Engineering and Applied Mechanics, University of Rhode Island, Kingston, RI 02881, U.S.A.

and

HARRY ZERVAS

Naval Undersea Warfare Center, Newport, RI 02841, U.S.A.

(*Received* 3 *February* 1994)

Abstract—An experimental study is conducted using dynamic photoelasticity and strain gage techniques to investigate transient stress fields in aggregate assemblies of circular disks. In particular, attention is focused on the effect of damage and damage growth in the particles on the dynamic load transfer process. The experimental data are analyzed to obtain the wave velocity, contact load profiles, peak load attenuation, wave dispersion and other changes in the stress fields as the dynamic load transfer process takes place. Both near and far field effects due to the presence of a flaw on the load transfer process are studied. The results show that the size and the orientation of the flaw greatly influence the load transfer process locally. However, in the far field the flaw only affects the attenuation of the peak loads without changing the wavelength of the loading pulse.

1. INTRODUCTION

A granular medium is discrete in nature, and its response under the application of explosive loading is a highly complex dynamic process involving the local microstructural arrangement of particles, their material properties and the contact mechanisms. These processes are best studied by performing simple controlled experiments in which the load transfer information is obtained for the whole assembly of particles and then using this information to develop numerical codes to predict load–time history in more complex assemblies. This paper describes the experimental portion of this study and investigates the dynamic load transfer process in granular assemblies where particle damage is present and/or created during the wave propagation process.

Damage in particulate media is interpreted as varying from small amounts of surface damage to the more severe case of particle fracture into two or more pieces. Slight surface damage produces negligible changes in the inter-particle dynamic contact response between adjacent grains. For the more severe cases of larger damage zones or granular fracture, considerable effects are noted in the attenuation rates since propagation energy is dissipated in the fracture process through the creation of new surfaces and in diffusion of particulate kinetic energy. Also, some of the energy is reflected back from the free surfaces of the open flaws.

The study of wave propagation in granular media is interesting because of its importance to many areas of technology such as soil mechanics, earthquake engineering, powder metallurgy and vibration isolation systems. Investigators have utilized aggregate assemblies of elastic particles interacting through contact mechanisms to model granular materials such as sand, rock, etc. Early work by Iida (1939), Takahashi and Sato (1949), Hughes and Cross (1952), Gassman (1951) and Brant (1955) employed a normal contact force concept, while Duffy and Mindlin (1957) included tangential forces as well. Some of the recent work in this field includes that of Thornton and Barnes (1986), Zhu *et al.* (1991),

Dvorkin *et al.* (1991), Ting and Corkum (1992), Shukla *et al.* (1993) and Sadd *et al.* (1993). Results of their efforts have led to initial attempts at predicting stress wave propagation in granular media. However, very few studies have been conducted to investigate media damage as it relates to wave propagation. Shin and Karr (1990) presented a one-dimensional wave propagation study of a viscoelastic medium with a continuum damage evolution model used for boundary and transgranular cracking of polycrystalline ice. A collection of articles in a book edited by Rossmanith (1983) outlines wave propagation in damaged blocky materials. Nonetheless little quantitative information exists on dynamic load transfer in damaged particulate materials.

This paper focuses on the effect of open flaws in particles on the dynamic load transfer process in particulate aggregates. Both dynamic photoelasticity and strain gages are utilized to collect stress and strain information in the bulk of the material and at contact points. The effect of flaws on the group wave propagating in the assembly is evaluated in terms of the peak contact load attenuation and wave dispersion. The results elucidate some of the basic mechanisms of energy dissipation and redistribution during the interaction of stress waves with flaws in particles.

2. PHOTOELASTIC EXPERIMENTS

2.1. *Experimental procedure*

A series of experiments was conducted on single chain assemblies of circular disks which were dynamically loaded by detonating a small amount of explosive lead azide directly on top of the assembly. Figure 1 shows such an assembly along with the explosive charge holder. The disks were machined from a brittle, transparent polyester material, Homalite 100, which is birefringent and ideally suited for photoelastic studies. One or more

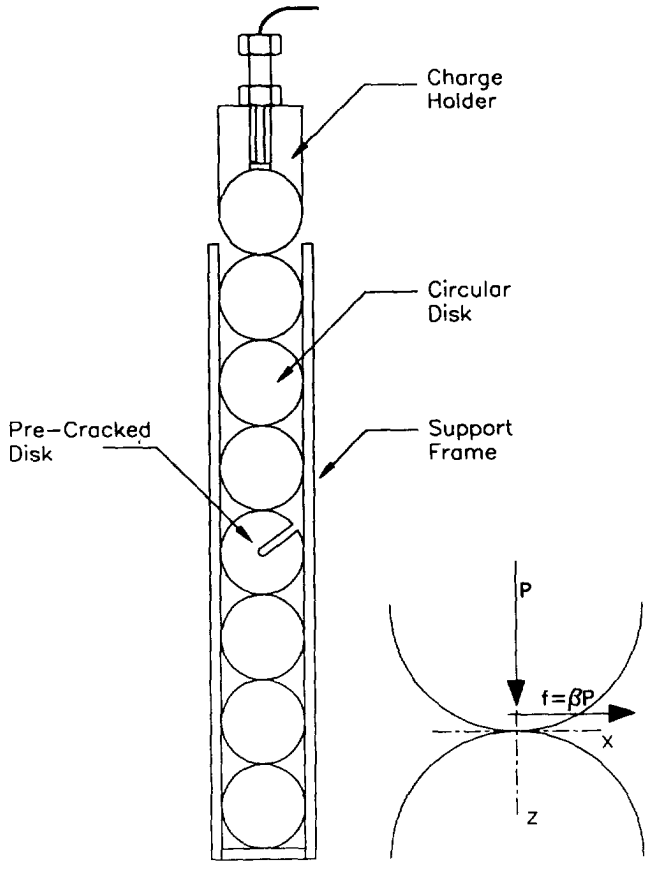

Fig. 1. Experimental setup for explosive loading of a single chain assembly containing a cracked disk.

disks with flaws were included in the chain. The flaw was simulated by an "open crack" which was machined using a band-saw. The assembly was placed in the optical bench of a multiple-spark, high-speed camera. An explosive charge of 20 mg was detonated in a specially designed charge holder. The camera was synchronized to record photographs after a predetermined time from the explosion. A series of intense flashes of light were generated by the camera providing 20 images during the experiment. A typical set of photographs obtained for a single chain assembly with no cracked disk, using this technique, is shown in Fig. 2. During the experiments the size and orientation of the crack were varied, and their effects on the wave propagation process studied.

2.2. *Analysis procedure*

The experimental data obtained were analyzed using the stress field equations developed by Smith and Liu (1953) coupled with a multipoint non-linear numerical technique proposed by Shukla and Nigam (1985). This technique uses full-field photoelastic data to evaluate the contact stresses and the contact area by utilizing the method of least-squares in conjunction with the Newton–Raphson method.

As shown in the coordinate system provided in Fig. 1, the disk is subjected to a normal distributed load of P N per unit length, which presses it against another disk over a narrow area of contact whose width is $2b$. A lateral distributed load of f N per unit length is also applied to the body. Let β be defined as the friction factor such that $f = \beta P$. β will be the coefficient of friction if motion impends. Neglecting far field effects, the stresses σ_{zz}, σ_{xx} and σ_{zx} for points close to the contact are given by

$$\sigma_{zz} = -\frac{b}{\pi\Delta}[z(b\phi_1 - x\phi_2) + \beta z^2\phi_2] \tag{1}$$

$$\sigma_{xx} = -\frac{b}{\pi\Delta}\left[z\left(\frac{b^2+2z^2+2x^2}{b}\phi_1 - \frac{2\pi}{b} - 3x\phi_2\right) + \beta\left((2x^2-2b^2-3z^2)\phi_2 + \frac{2\pi x}{b} + 2(b^2-x^2-z^2)\frac{x}{b}\phi_2\right)\right] \tag{2}$$

$$\sigma_{zx} = -\frac{b}{\pi\Delta}\left[z^2\phi_2 + \beta\left((b^2+2x^2+2z^2)\frac{z}{b}\phi_1 - 2\pi\frac{z}{b} - 3xz\phi_2\right)\right], \tag{3}$$

where ϕ_1 and ϕ_2 are defined as

$$\phi_1 = \frac{\pi(M+N)}{MN\sqrt{(2MN+2x^2+2z^2-2b^2)}}$$

$$\phi_2 = \frac{\pi(M-N)}{MN\sqrt{(2MN+2x^2+2z^2-2b^2)}}$$

$$M = \sqrt{[(b+x)^2+z^2]}, \quad N = \sqrt{[(b-x)^2+z^2]}$$

$$\Delta = \frac{2R(1-\nu^2)}{E},$$

where R is the radius of curvature at the point of contact, E is the modulus of elasticity and ν is the Poisson's ratio. The two unknowns in the stress field equations are b and β. Other parameters depend on the geometry of the bodies, location coordinates and material properties. Equations (1)–(3) are coupled with the stress optic law (Shukla and Nigam, 1985), and the two unknowns, namely the half contact length b and the friction factor β,

are obtained from the photoelastic data. The stresses thus obtained are integrated to give the contact loads. The wave velocity is obtained by plotting the stress wave front as a function of time. The wavelength of the stress wave pulse is obtained directly from the photographs as shown in Fig. 2. Wave dispersion information is obtained from the load–time profile. The experiment shown in Fig. 2 was used for comparison with experiments with flawed particles.

3. STRAIN GAGE EXPERIMENTS

3.1. *Experimental procedure*

Dynamic photoelasticity, in conjunction with high speed photography, allows for full-field visualization and analysis of the stress wave pulse. However, the limited field view of the camera places restriction on the number of disks that can be observed in one experiment. Strain gages (MicroMeasurements: EA-13-031DE-120) were used to observe the far field effects of including a flawed particle in a long chain assembly of disks. The experimental setup is shown in Fig. 3. The single chain assembly of disks was loaded explosively as in the photoelastic experiments. Eight separate strain gages, at various locations, were used to monitor the strains resulting from the stress wave propagating in the assembly. The first four strain gages were located at contact points around the cracked disk (disk number 13), as shown in Fig. 3. The other gages were located at various contacts further down the single chain assembly. Data collection and storage was accomplished by dynamic Ectron amplifiers and a Lecroy digital data acquisition system. The frequency response of these systems was adequate for the stress wave propagation experiments. Figure 4 shows the strains measured for a single chain assembly containing no flawed particles. This experiment also served as the baseline experiment, for comparison purposes.

3.2. *Analysis procedure*

For the case of plane stress,

$$\varepsilon_{zz} = \frac{1}{E}(\sigma_{zz} - \nu\sigma_{xx}). \tag{4}$$

Hence, from the stress field equations developed by Smith and Liu (1953), the strain ε_{zz}, along the z-axis ($x = 0$), for $\beta = 0$, is given as,

$$\varepsilon_{zz} = -\frac{1}{E}\left[\frac{(1-\nu)b^2 - 2\nu z^2}{\Delta\sqrt{(b^2+z^2)}} + \frac{2\nu z}{\Delta}\right]. \tag{5}$$

Using strain gage data, the half contact length, b, is determined from eqn (5). Once this parameter is known, the stresses and the normal contact load are determined as discussed in Section 2.2. The velocity and wavelength of the stress wave pulse are determined directly from the strain versus time data.

4. RESULTS AND DISCUSSION

The results obtained from the series of experiments to study the effect of damage and damage growth on dynamic load transfer in particulate media are discussed in the following sections.

4.1. *Effect of crack length*

A series of dynamic photoelastic experiments were conducted to observe the near field effects of crack length on the stress wave propagation through granular media. In all, three different crack lengths were used and each experiment contained a single flawed particle. The results from all these experiments were analyzed to study the effect of the crack length on dynamic load transfer characteristics, in particular, on the attenuation, dispersion and

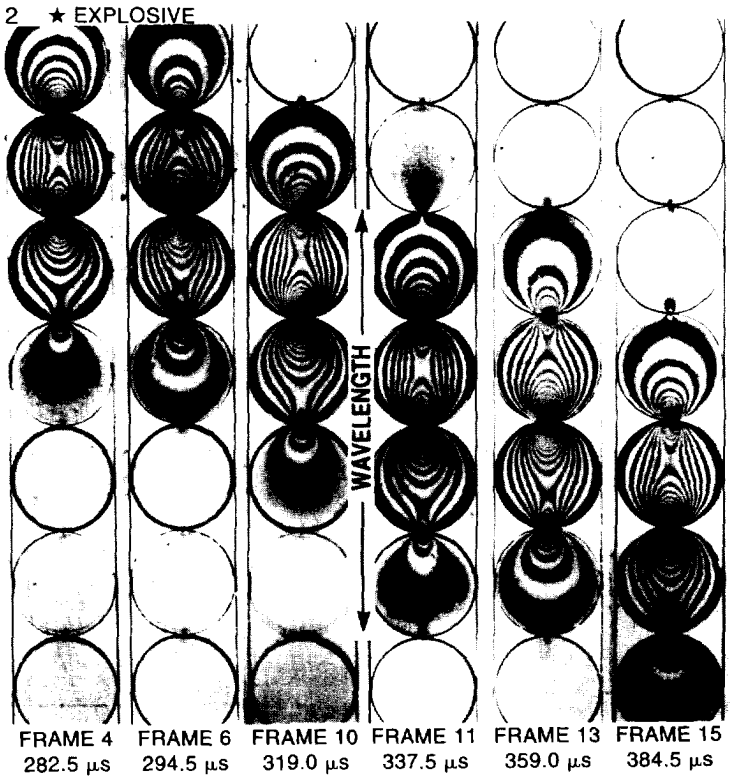

Fig. 2. Typical isochromatic fringes obtained for a single chain assembly with no cracked disk.

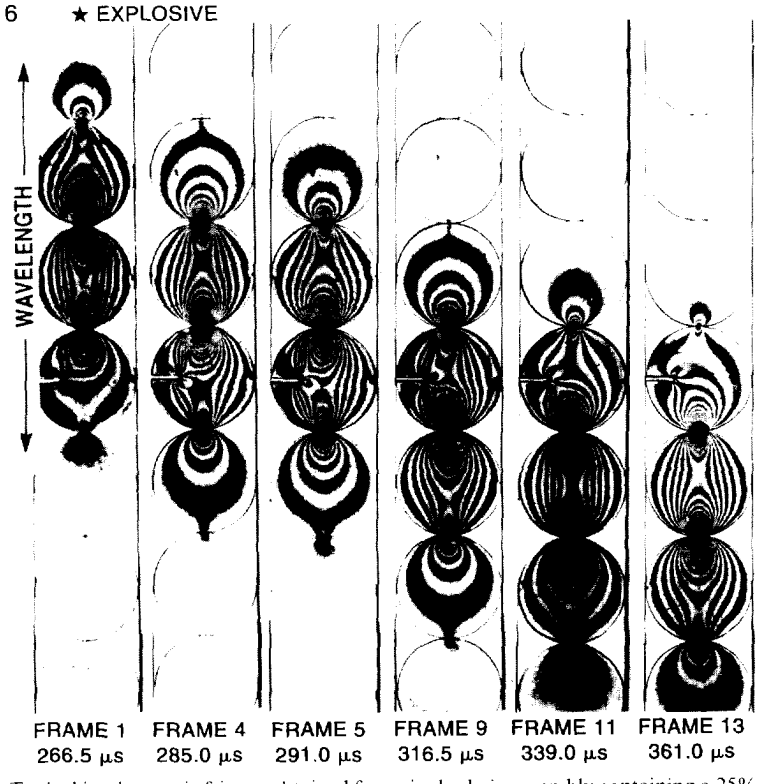

Fig. 6. Typical isochromatic fringes obtained for a single chain assembly containing a 25% cracked disk.

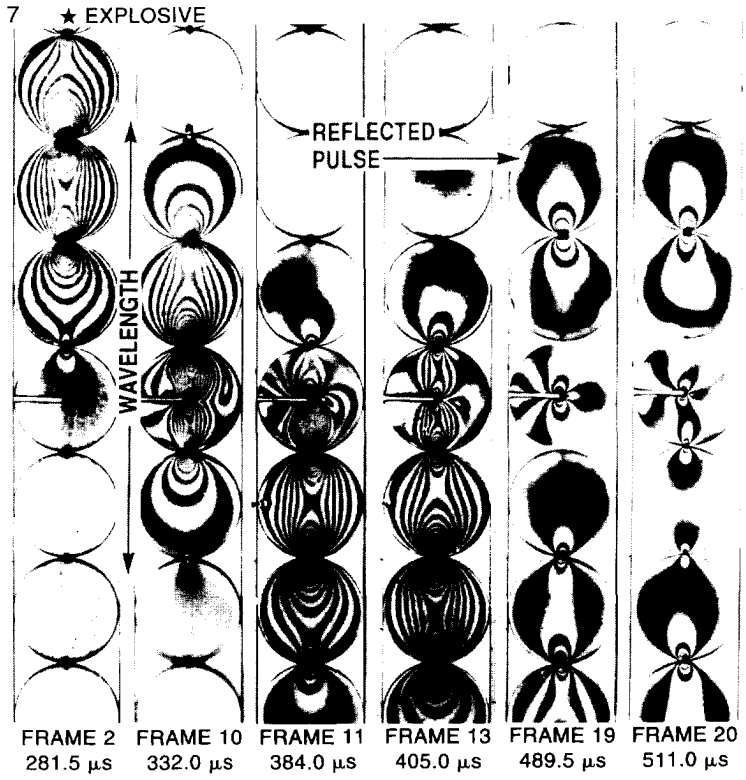

Fig. 7. Typical isochromatic fringes obtained for a single chain assembly containing a 50% cracked disk.

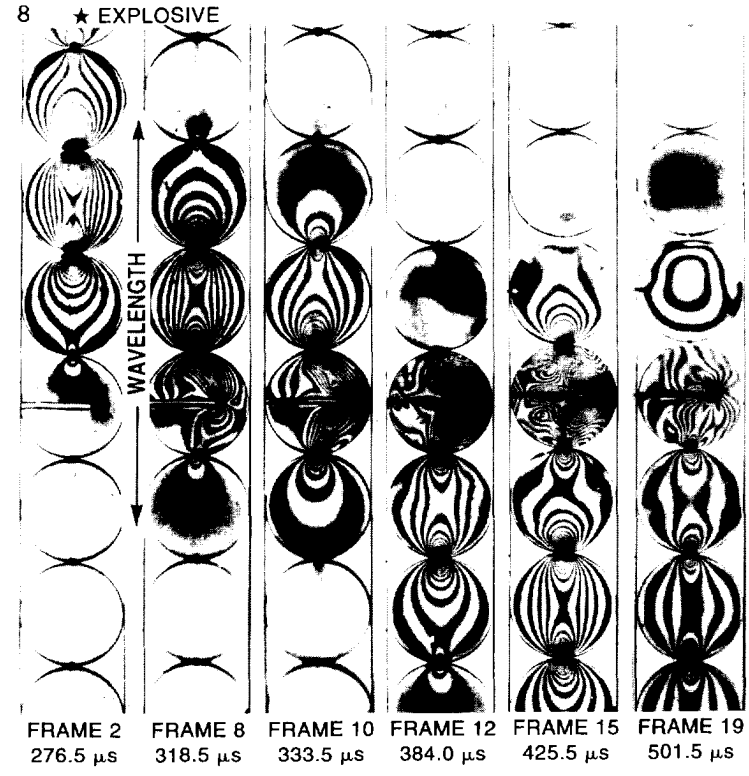

Fig. 8. Typical isochromatic fringes obtained for a single chain assembly containing a 75% cracked disk.

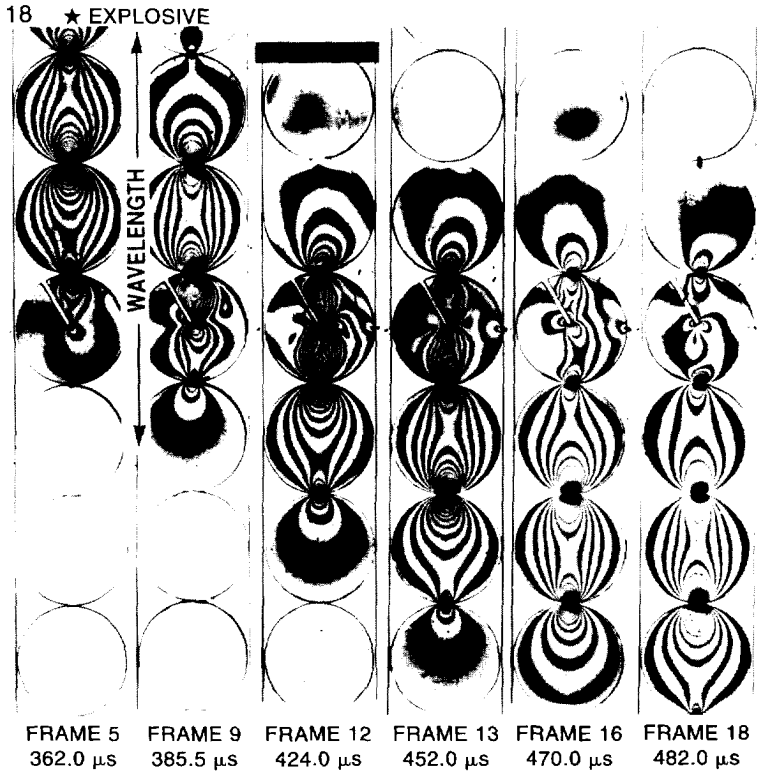

Fig. 18. Typical isochromatic fringes obtained for a single chain assembly containing a 50% cracked disk oriented at +60 .

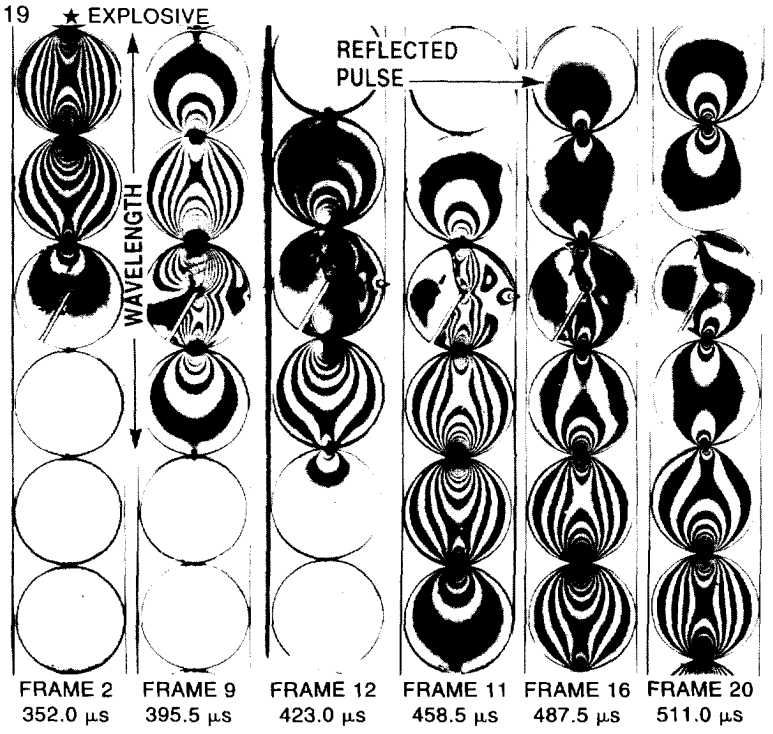

Fig. 19. Typical isochromatic fringes obtained for a single chain assembly containing a 50% cracked disk oriented at −60 .

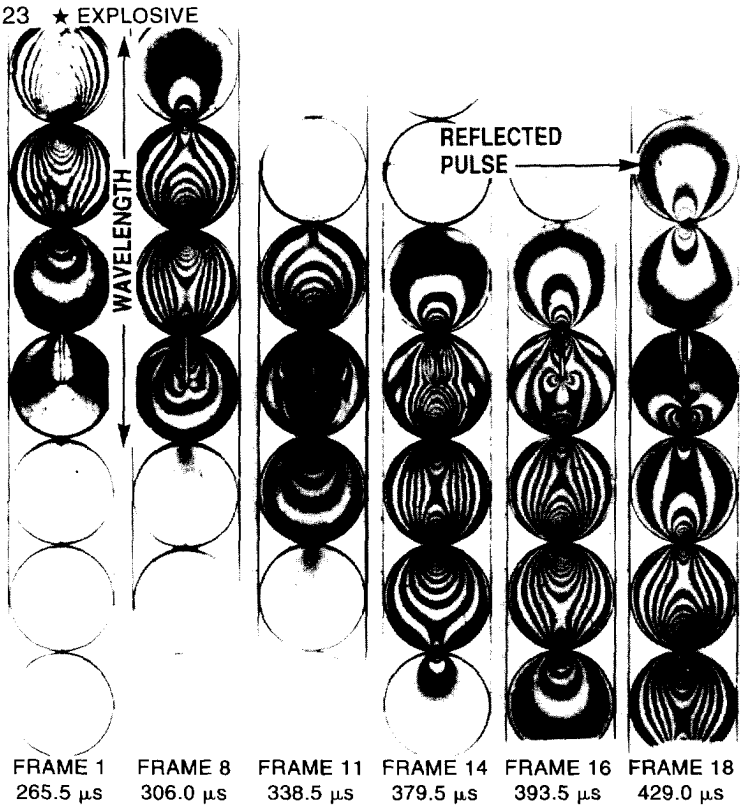

Fig. 23. Typical isochromatic fringes obtained for a single chain assembly containing a 50% cracked disk oriented at +90 .

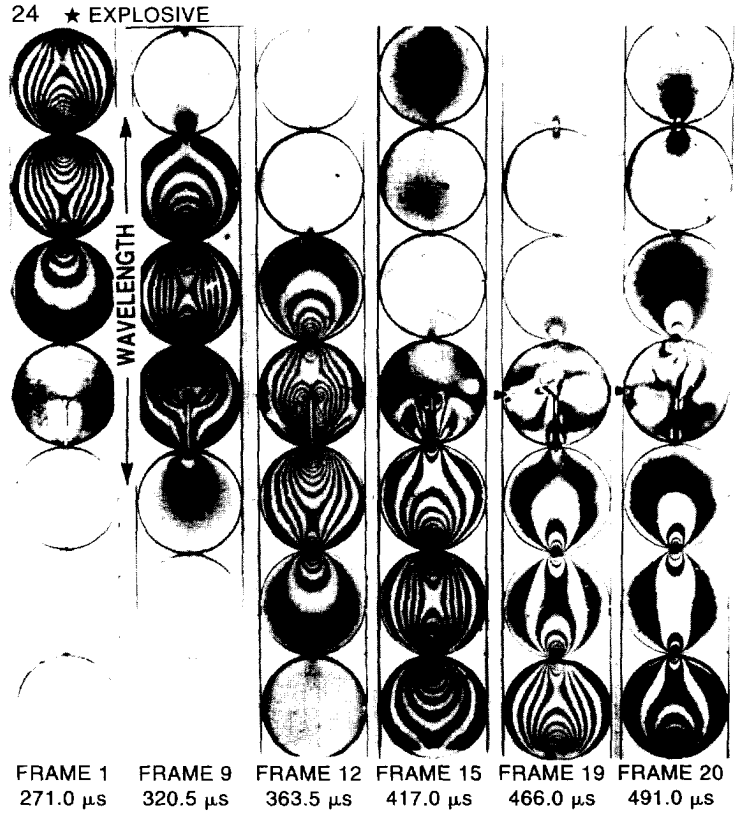

Fig. 24. Typical isochromatic fringes obtained for a single chain assembly containing a 50% cracked disk at −90 .

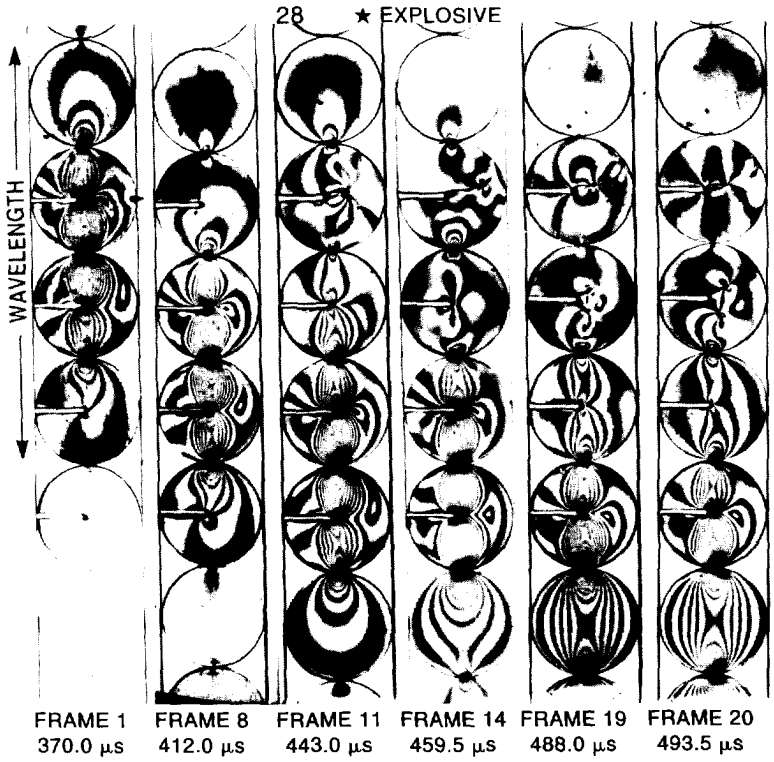

Fig. 28. Typical isochromatic fringes obtained for a single chain assembly containing multiple cracked disks with aligned cracks.

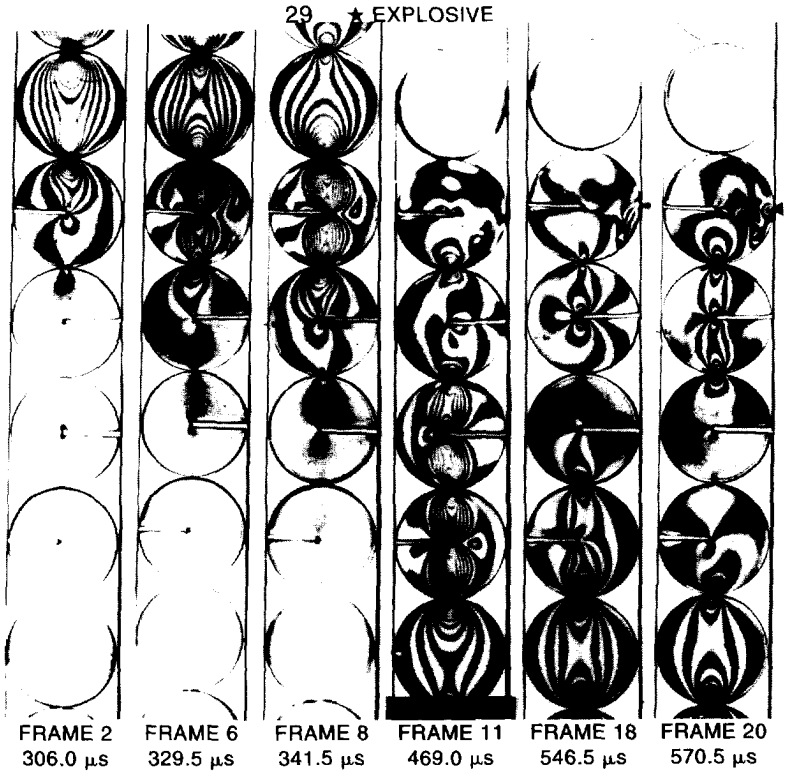

Fig. 29. Typical isochromatic fringes obtained for a single chain assembly containing multiple cracked disks with staggered cracks.

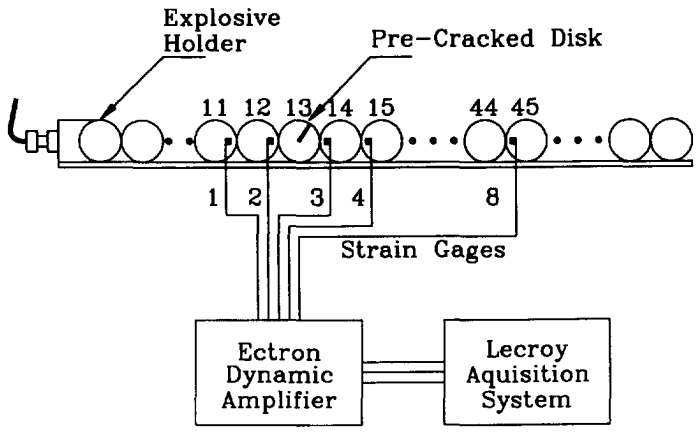

Fig. 3. Experimental setup for long chain experiments using strain gages.

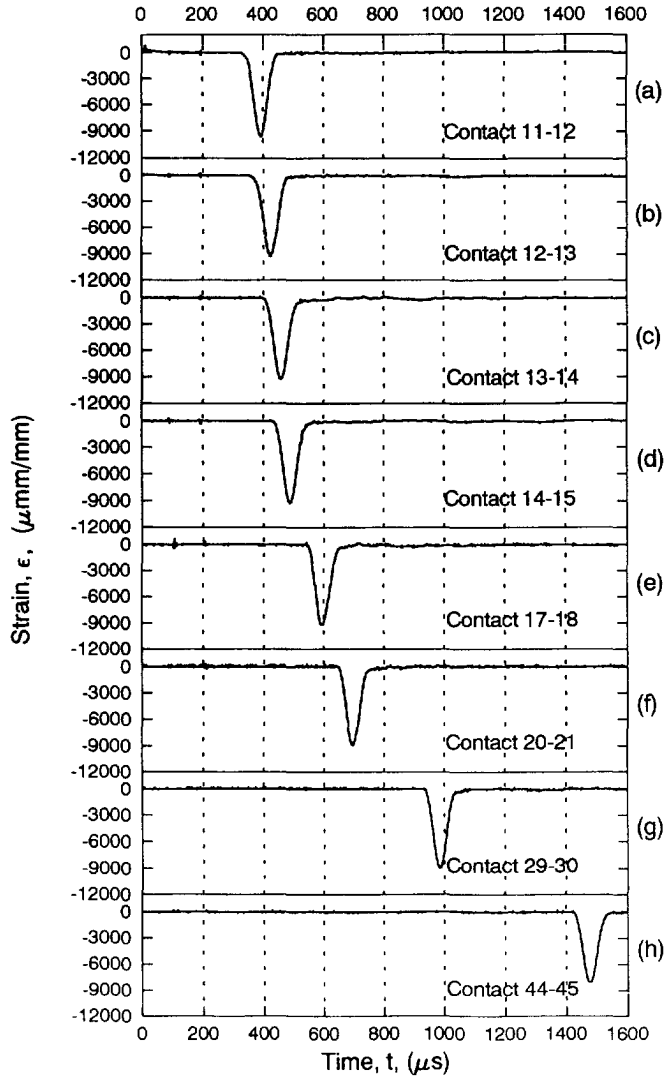

Fig. 4. Strain gage data for a single chain assembly with no cracked disk.

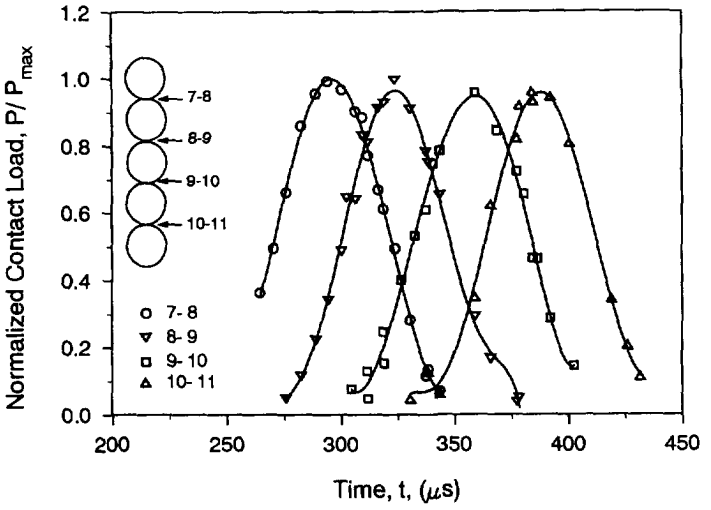

Fig. 5. Variation of normal contact loads as a function of time for a single chain assembly containing no cracked disk.

wave propagation speed. The crack length was varied from 0 to 75% of the disk diameter in increments of 25%. In all of the cases, the cracked disk was oriented such that the crack was parallel to the tangent plane of contact.

Typical isochromatic fringes obtained for a single chain assembly with no cracked disk are shown in Fig. 2. These photographs were analyzed, and the contact load profiles obtained as a function of time are shown in Fig. 5. As shown by this figure, the stress wave propagated through the assembly with no dispersion and negligible load attenuation. The average wave velocity and wavelength were determined to be 1050 m s^{-1} and four disk diameters, respectively. Both remained constant throughout the propagation of the wave. Consequently each contact point was loaded for about 100 μs.

A series of typical isochromatic patterns obtained for the 25, 50 and 75% crack assemblies are shown in Figs 6, 7 and 8, respectively. These photographs clearly indicate that the crack influenced stress wave propagation and also the stress field distribution within the cracked disk. However, the nature of the stress field in the uncracked disks was not affected, and the Hertz contact theory, as discussed before, could still be used for analysis. The contact load profiles obtained from these experiments are shown in Figs 9–

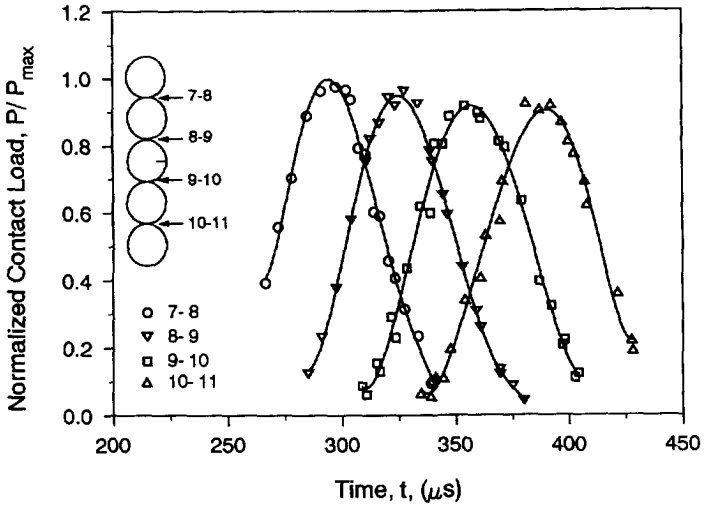

Fig. 9. Variation of normal contact loads as a function of time for a single chain assembly containing a 25% cracked disk.

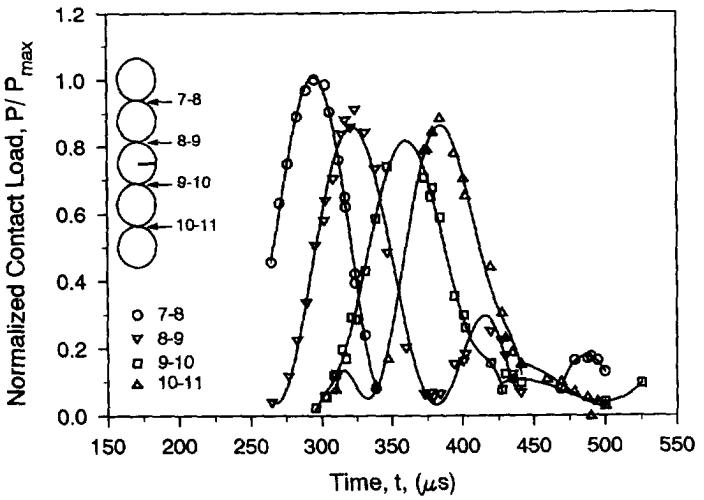

Fig. 10. Variation of normal contact loads as a function of time for a single chain assembly containing a 50% cracked disk.

11. The effect of the crack on the dynamic load transfer characteristics became more pronounced as the crack length was increased. The presence of a crack not only influenced existing load transfer mechanisms from particle to particle but also introduced some new mechanisms. Some of these effects are discussed in detail below.

As the stress wave encountered the cracked disk both reflection off the free surfaces of the open crack and scattering at the crack tip took place. When compressive parts of the stress wave pulse impinged on the free surface of the crack, they were reflected as tensile. These tensile reflections interacted with the preceding contact. As a result, part of the compressive loading at this contact was neutralized, and energy was transmitted back up the chain. This resulted in a 25% attenuation in the contact load at the preceding contact (for the 75% crack case) even before the pulse had propagated through the cracked disk. The energy transmitted back up the chain was observed as a back reflected pulse as shown in the nineteenth and twentieth frames in Fig. 7.

The interaction of the stress wave with the crack also resulted in dynamic loading of the crack. The nineteenth frame in Fig. 7 shows typical isochromatic fringes in the cracked disk as one would expect for a crack under mode I loading. The dynamic nature of this loading was evident from the lack of any contact stresses between the cracked disk and its adjoining disks. For the 75% crack case, interaction of the stress wave with the crack

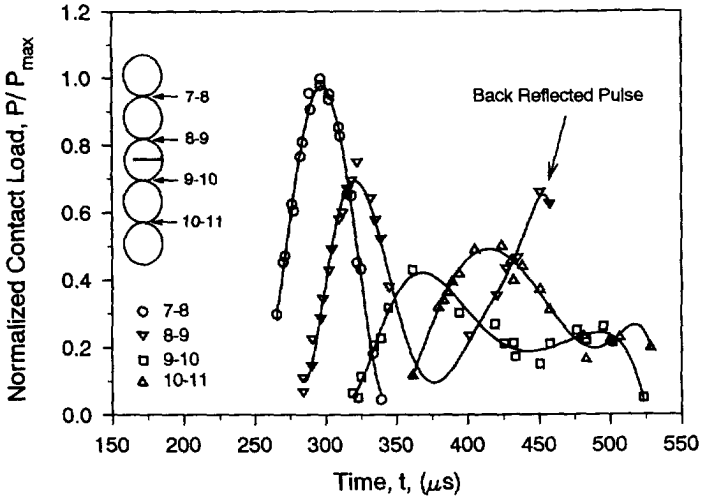

Fig. 11. Variation of normal contact loads as a function of time for a single chain assembly containing a 75% cracked disk.

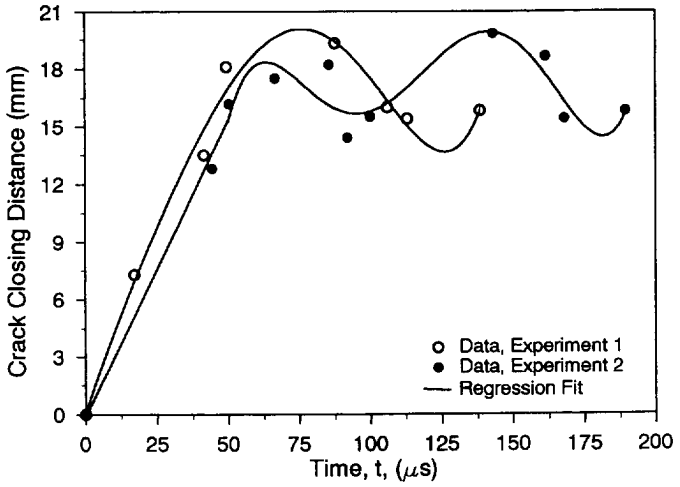

Fig. 12. Crack closing distance as a function of time, for dynamic loading of a disk with a 75% disk diameter crack.

resulted in extremely high stresses within the cracked disk as shown by the high density of isochromatic fringes in the twelfth, fifteenth and nineteenth frames in Fig. 8. These high stresses resulted in crack closure causing the crack surfaces to come into contact. Rapid closure of the crack surface for two 75% crack experiments is plotted in Fig. 12. The crack closed to 80% of its total length at a rapid rate of 450 m s^{-1}. This crack closure speed is higher than the terminal crack speeds observed normally in this material. The crack remained partially closed for the duration of the experiment, and exhibited oscillations in the closure length. The oscillations were expected because of the oscillatory nature of the stress field.

The crack behaved as a barrier, blocking the path of the stress wave pulse. As the crack closed, for example in the 75% crack case, some energy was allowed to transfer across the contacting crack surfaces. However, most of the stress wave was subjected to many more reflections within the cracked disk before it could reach the next contact point. These multiple reflections resulted in elongation of the stress wave pulse. As the pulse propagated through the cracked disk, it elongated from an input duration of 90 μs to a much greater duration. The complete elongated pulse was not observed in the photoelastic experiments because of the limited field of view of the camera. Varying the crack length had no effect on the average velocity of the stress wave pulse. This is consistent because the group wave velocity for a given particulate media depends primarily on the contact geometry.

A series of strain gage experiments was conducted with the same assemblies to observe wavelength elongation and peak load attenuation of the stress wave as it propagated through the cracked disk. Figures 13–15 show the strain versus time plots for a single chain assembly containing 25, 50 and 75% cracked disks. Many new features were observed in these experiments. In addition, certain features observed in the photoelastic experiments were also confirmed, such as the presence of a strong back reflected pulse. The back reflected pulses, for the 75% crack case, are shown in Figs 15(a), (b). Similar features were observed in all the experiments. For brevity only the results from the 75% crack assembly are presented as follows.

As the stress wave pulse passed through the cracked disk (disk number 13) many non-linear stress wave effects were observed. The duration of the loading pulse was almost tripled from 120 to 330 μs. Moreover, the pulse profile immediately following the cracked disk was jagged and rough [see Fig. 15(c)] as compared with the smooth input pulse. The jaggedness of the pulse profile was a result of increased reflections that the stress wave was subjected to as it propagated through the cracked disk. These perturbations in the pulse were an indication of high frequency components now present in the wave profile. Some of these high frequency components were rapidly dissipated by the granular medium resulting in smoothening of the elongated pulse profile. This occurred as soon as the pulse propagated

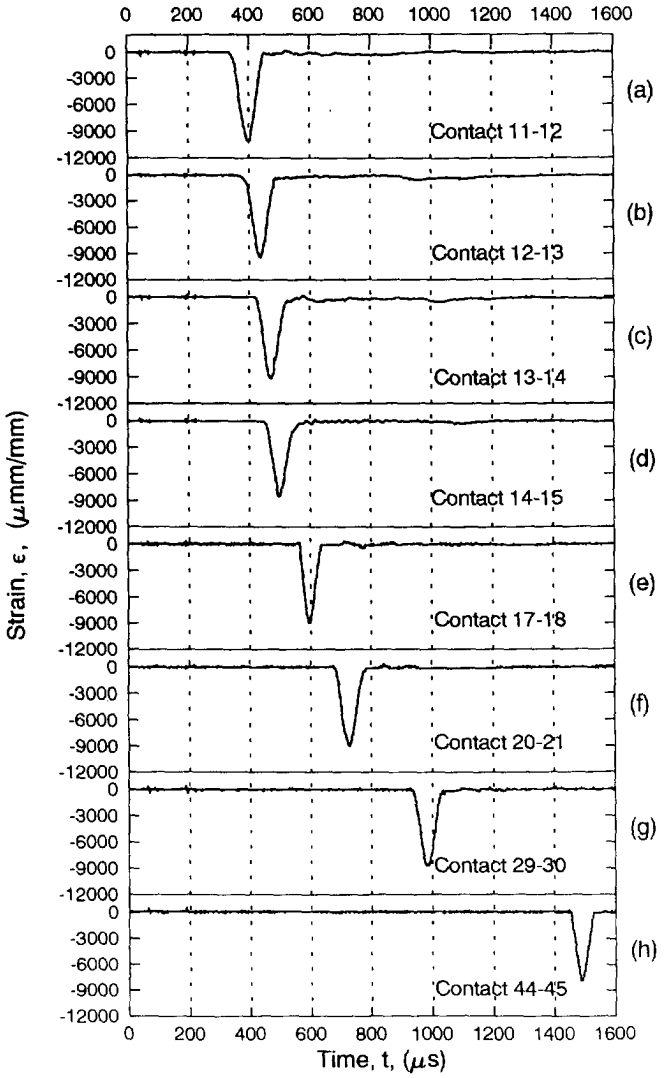

Fig. 13. Strain gage data for a single chain assembly containing a 25% cracked disk.

through a single disk, as evidenced by the much smoother profile shown in Fig. 15(d). The elongated pulse shown in Fig. 15(d) had a duration of 360 μs, which represented 12 disk diameters. As this elongated pulse propagated further, it quickly separated into four wavelets with average peak separations of 90 μs [see Figs 15(d–f)]. The separation of the elongated pulse into several wavelets was a result of redistribution of energy associated with a ringing phenomenon which produces oscillations within a long wavelength pulse. During this redistribution of energy the primary wavelet gathered some of the energy from the elongated pulse and registered an increase in amplitude. The separation between the various wavelets increased with propagation distance as the wavelets travelled with different velocities. As shown in Fig. 16 the average velocity decreased from 950 m s^{-1} for the first wavelet to 760 m s^{-1} for the fourth wavelet. The separated wavelets had a specific wavelength to disk diameter ratio of about four, which was equivalent to the wavelength of the input pulse. This implies that this single chain assembly can support only those stress wave pulses that have a wavelength to disk diameter ratio of about four. Stress wave pulses with such a wavelength propagate with no dispersion and small attenuation, whereas longer wavelengths separate into wavelets with the same specific wavelength to disk diameter ratio of about four. With further propagation down the single chain assembly, the secondary wavelets were rapidly dissipated resulting in a far field stress wave pulse that resembled the

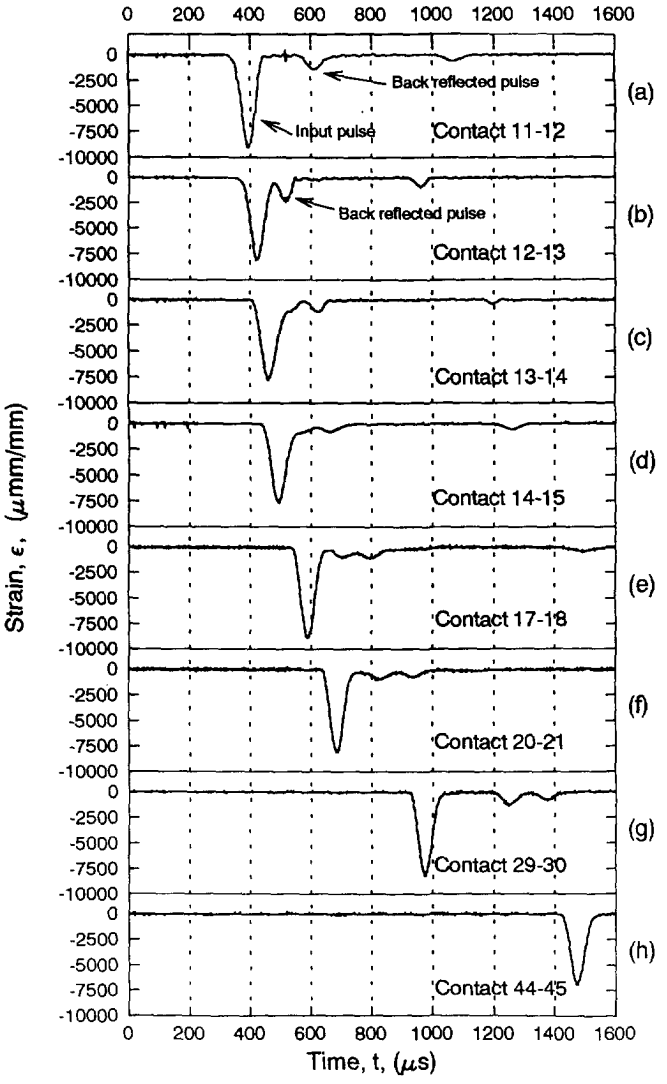

Fig. 14. Strain gage data for a single chain assembly containing a 50% cracked disk.

input pulse. The property of a single chain assembly to support only those pulses with a specific wavelength to disk diameter ratio of four can be explained in terms of the modal characteristics of the granular medium. This phenomenon has been observed earlier and the details are presented by Shukla *et al.* (1993).

The inclusion of a cracked disk in the single chain assembly resulted in large far field attenuation of the peak contact load. Figure 17 shows the peak contact load attenuation as a function of distance propagated. The peak contact load attenuation increased from 20% for the no crack case to 55% for the 75% crack case in a 1 m distance of travel. This increase in attenuation was a result of energy being reflected back up the chain and energy being lost from the dissipation of secondary wavelets. Figure 17 also shows the local drop in the peak contact load due to pulse elongation and subsequent increase in the peak contact load associated with the ringing phenomenon.

The average velocity of the stress wave pulse was determined to be 950 m s^{-1}, for all the crack assemblies, which remained constant throughout the propagation of the stress wave pulse. This was in good agreement with the photoelastic data.

4.2. *Effect of crack orientation*

A series of dynamic photoelastic experiments was conducted to observe the near field effects of crack orientation on stress wave propagation through granular media. To

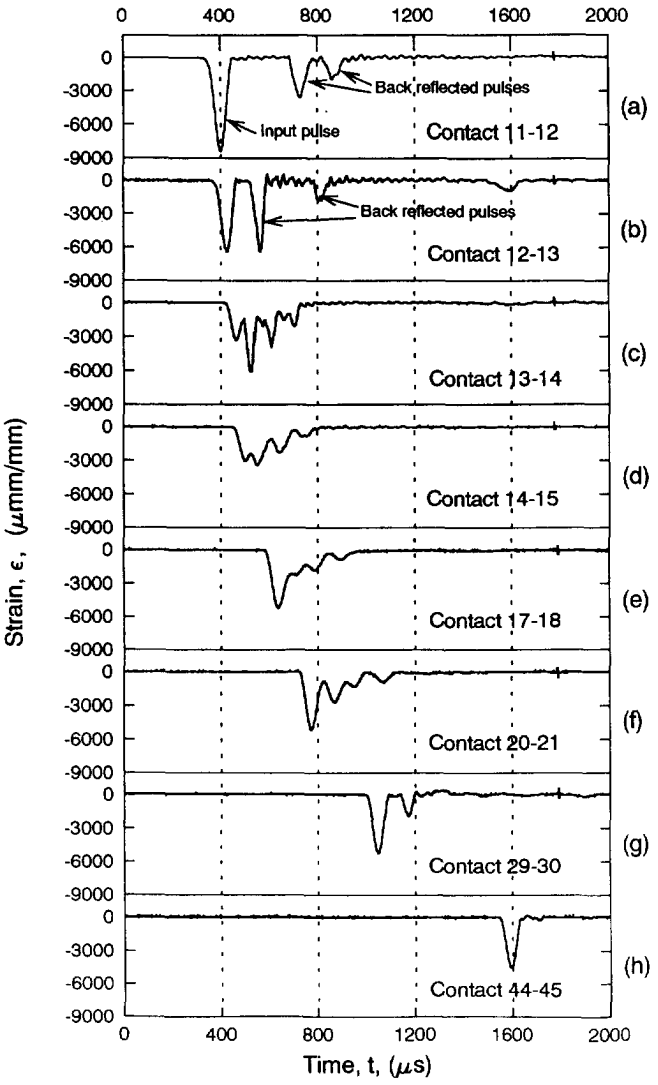

Fig. 15. Strain gage data for a single chain assembly containing a 75% cracked disk.

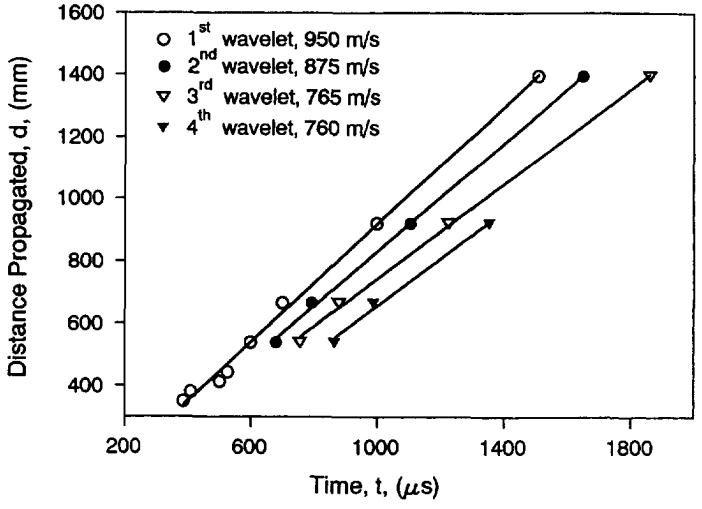

Fig. 16. Distance propagated as a function of time by the various wavelets.

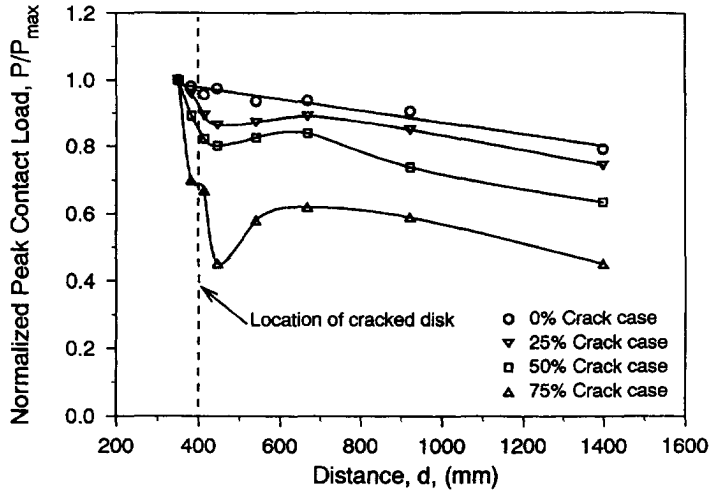

Fig. 17. Load attenuation as a function of distance propagated for explosive loading of single chain assemblies containing disks with various crack lengths.

investigate the dynamic load transfer characteristics, seven different single chain assemblies were studied. The crack orientation was varied from $-90°$ to $+90°$ in increments of 30°, where the angle was measured from the tangent plane of contact. In all the assemblies, the crack length was maintained constant at 50% of the disk diameter.

Typical isochromatic fringes obtained for the $-60°$ and $+60°$ crack orientations are shown in Figs 18 and 19, respectively. As observed in earlier experiments, the presence of a crack influenced stress wave propagation through the assembly. However, in crack orientation assemblies, the relative angle of the crack with respect to the incoming stress wave pulse also influenced the interaction of the stress wave with the crack surfaces and the crack tip. For the $+60°$ orientation, the incoming stress wave pulse interacted with the crack surface at grazing incidence, causing both longitudinal and shear waves to be reflected off the crack surface. The shear component in the reflections was substantial due to the specific angle of inclination of the crack. Interaction of these shear waves, with the preceding contact, resulted in an oscillatory shear loading at the contact as evident from the change in the tilt of the isochromatic fringes shown in Fig. 18. The shear loads at the preceding contact were calculated and are plotted in Fig. 20, for two separate experiments. The magnitude of the shear loading was quite large with its peak value equal to about 20% of the peak normal load. The results also confirmed the oscillatory nature of the shear

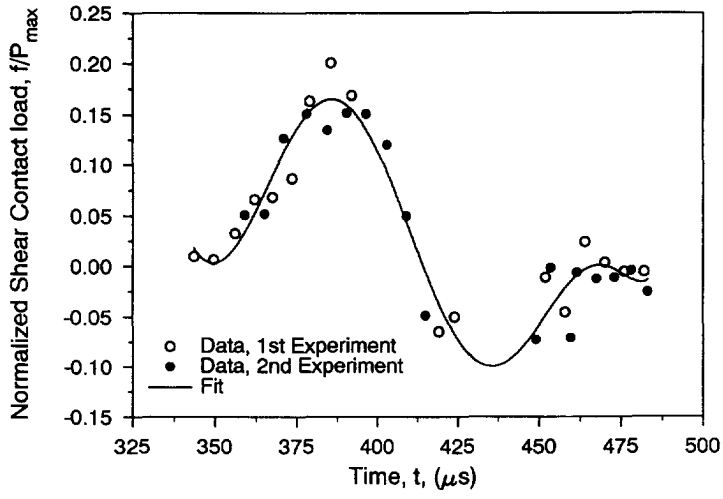

Fig. 20. Variation of shear load at contact preceding the cracked disk for explosive loading of a single chain assembly contain a 50% cracked disk oriented at $+60°$.

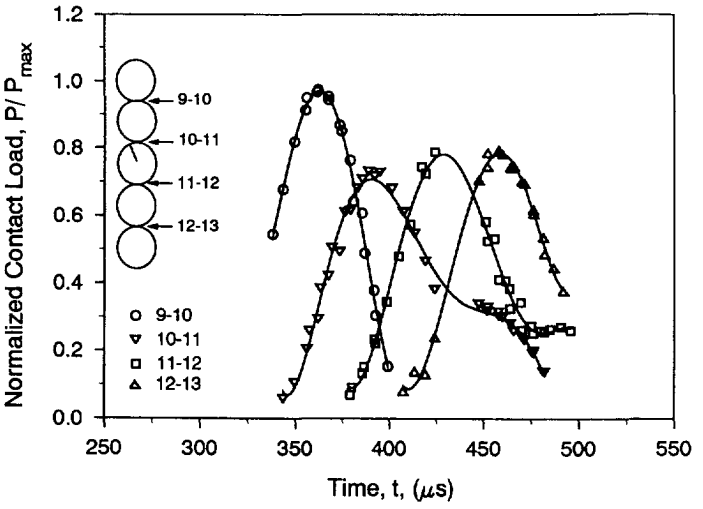

Fig. 21. Variation of normal contact loads as a function of time for a single chain assembly containing a 50% cracked disk oriented at +60°.

reflections coming back to the contact point. However, shear loading of the preceding contact was not observed for the −60° orientation case, because of the relative angle of impingement of the stress wave with the crack surfaces.

Interaction of the stress wave pulse with the crack resulted in loading of the crack tip. However, unlike the horizontal case experiments the angled cracks were subjected to mixed mode loading, as observed from the crack tip isochromatic fringes in Figs 18 and 19. Moreover, the relative angle of the crack, with respect to the stress wave pulse, governed the nature of stresses at the crack tip. For cracks oriented away from the incoming stress wave pulse, as for the +60° case, most of the reflections occurred only from one surface of the open crack. However, for cracks oriented towards the incoming stress wave pulse, as for the −60° case, reflections occurred from both crack surfaces. Also, the more direct impingement of the stress wave on the crack tip for the −60° case resulted in sufficiently high tensile stresses at the crack tip to cause crack growth, as shown in the ninth, tenth and eleventh frames in Fig. 19. The crack in this case was initiated even before the peak of the stress wave pulse had reached the cracked disk. The average crack velocity was determined to be 260 m s^{-1}. Post-experimental observations indicated a smooth crack surface, which corresponds to a dynamic stress intensity factor, K_{ID}, of about 0.5 MPa $m^{1/2}$ for this material. The energy dissipated in the growth of this crack was determined to be 7×10^{-3} J, which was at least an order of magnitude lower than the total energy of the stress wave pulse. Thus, even though crack growth did not result in significant energy dissipation, it caused significant microstructural changes in the granular medium. As shown in the sixteenth and twentieth frames in Fig. 19, the fractured particle had already separated from the single chain assembly by rigid body motion even before the pulse had propagated through the single chain assembly. The various features discussed above were also observed, to a lesser degree, for the +30° and −30° crack orientations. For the sake of brevity, the results from these experiments are not presented.

Despite the new features introduced as a result of varying the crack angle, the nature of the stress field in the uncracked disks was not affected, and the Hertz contact theory could still be used for analysis. The contact load profiles obtained for the +60° and −60° crack orientation experiments are shown in Figs 21 and 22, respectively. Cracks oriented away from the incoming stress wave pulse returned more energy up the single chain assembly than cracks oriented towards the incoming stress wave pulse. This resulted in a 25% attenuation in the peak contact load at the preceding contact for the +60° case compared with only 5% for the −60° case. The energy reflected back up the chain was also observed as a back reflected pulse as shown in the sixteenth and twentieth frames in Fig 19.

The crack orientations of +90° and −90° represented special cases of the angled crack experiments. The cracks in these cases were oriented such that one of the contacts occurred

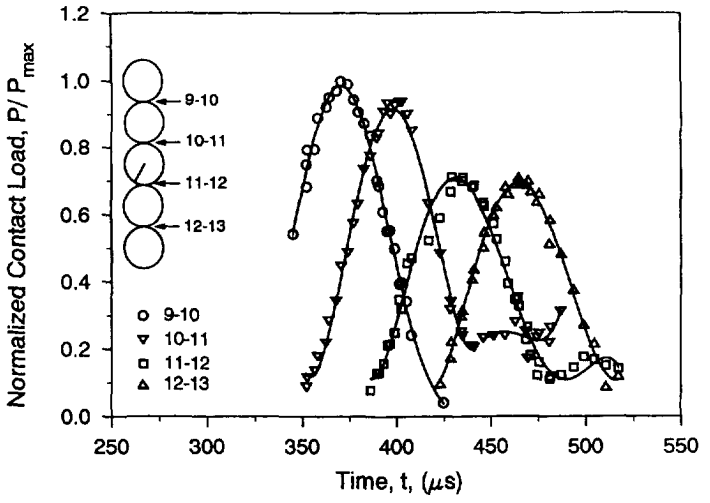

Fig. 22. Variation of normal contact loads as a function of time for a single chain assembly containing a 50% cracked disk oriented at -60°.

at the open end of the crack resulting in a two-point contact. Consequently, energy transfer across this contact occurred via two separate paths, as shown in the first frame in Fig. 23 and the ninth frame in Fig. 24. Moreover, as the crack surfaces were oriented along the direction of the incoming stress wave pulse, the direct reflections off the crack surfaces were minimized. The stress wave pulse impinged on the crack surfaces only after reflecting off the free boundaries of the cracked disk. These reflections were tensile in nature and were neutralized by the incoming compressive stress wave pulse. Consequently, the crack tips were not loaded until most of the stress wave pulse had propagated through the cracked disk, as shown in Figs 23 and 24. After the stress wave pulse had passed through the cracked disk the tensile reflections became dominant causing opening mode loading of the crack tip and subsequent crack growth. Such crack growth was observed for both the orientations. Moreover, the tensile stresses for the -90° case were high enough to cause crack branching. The average velocity of the crack for the $+90^{\circ}$ case was determined to be 300 m s^{-1}. For the -90° case the crack velocities were determined to be 300 m s^{-1} and 100 m s^{-1}. The slower crack did not have enough energy to propagate and arrested during the experiment. The crack surfaces for the cracks that propagated through the disk were observed to be smooth, as expected.

As for the previous cases, the isochromatic fringes were analyzed and the contact load profiles for the $+90^{\circ}$ and -90° cases are shown in Figs 25 and 26, respectively. The peak contact load attenuation, at contact preceding the cracked disk, was 25% for the $+90^{\circ}$ case as compared with only 10% for the -90° case. This was again due to the same reasons as discussed for the $+60^{\circ}$ and -60° crack orientation experiments.

Pulse elongation was also observed for all the crack orientations, and once again strain gage experiments were conducted to determine the elongation of the pulse as it propagated through the cracked disk. The duration of the stress wave pulse increased from 120 to 200 μs, for the $+60^{\circ}$ and $+90^{\circ}$ orientations, and from 120 to 170 μs, for the -60° and the -90° orientations, as the pulse propagated through the cracked disk. Thus, there was no significant influence of the crack orientation on the elongation of the stress wave pulse. As this elongated pulse propagated down the chain it was also decomposed into wavelets. The secondary wavelets were dissipated and finally a wave with a characteristic wavelength to disk diameter ratio of four propagated down the assembly. Also the overall attenuation did not change significantly with variation in crack orientation, as shown in Fig. 27. The overall average attenuation in peak contact load was observed to be 35% for all the crack orientations for a propagation distance of 1 m.

Although the different orientations of the crack did not influence the overall attenuation of the peak contact load, they had a considerable effect on the resulting microstructure of the media. The cracks oriented towards the wave always resulted in the fracture of the

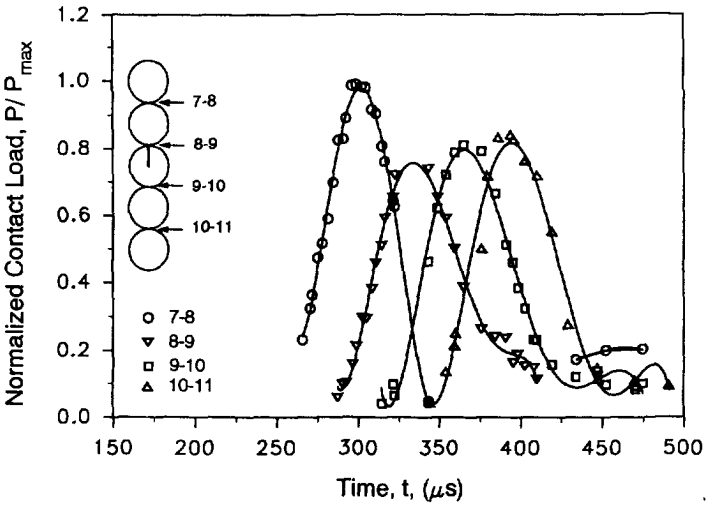

Fig. 25. Variation of normal contact loads as a function of time for a single chain assembly containing a 50% cracked disk oriented at +90°.

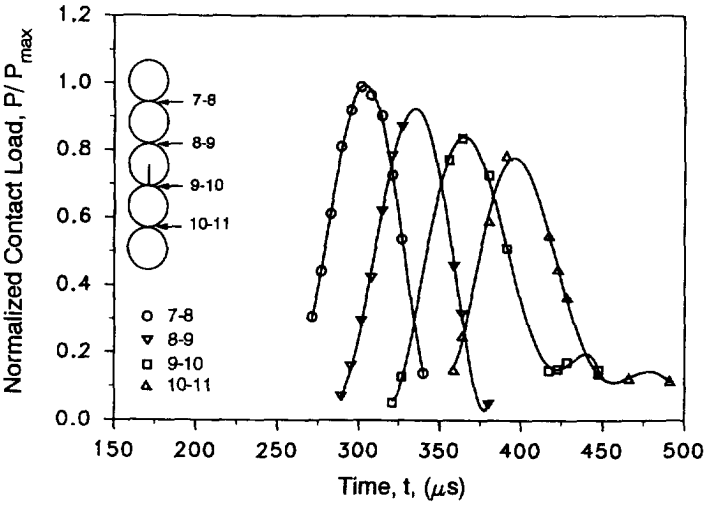

Fig. 26. Variation of normal contact loads as a function of time for a single chain assembly containing a 50% cracked disk oriented at −90°.

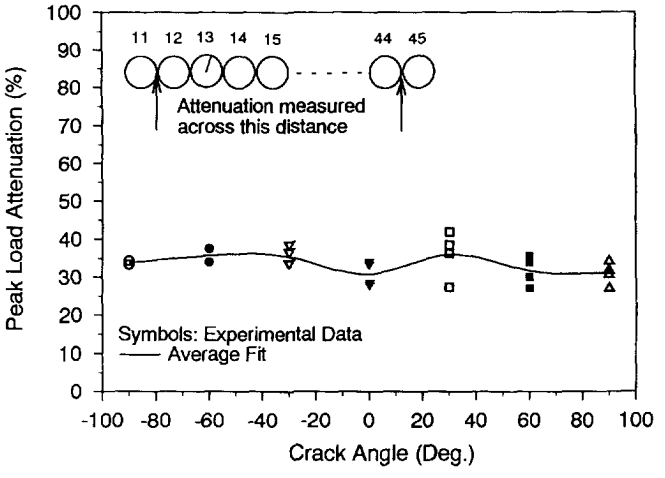

Fig. 27. Overall peak contact load attenuation as a function of crack orientation.

particles unlike the cracks oriented away from it. This would greatly affect the subsequent loadings of the media and also loadings from any reflected pulses from the far field boundaries of the container.

4.3. *Effect of multiple cracks*

A series of experiments was also conducted to investigate the effect of including more than one cracked disk in the single chain assembly. In these experiments four 50% cracked disks were placed adjacent to each other. The choice of four disks was based on the wavelength of the loading pulse in the media. Two separate arrangements were investigated; one with all cracks aligned in the same direction and another with cracks aligned in a staggered fashion. Typical isochromatic fringes obtained for these experiments are shown in Figs 28 and 29. As observed from these figures, substantial energy storage occurred within the cracked disks even after the stress wave pulse had propagated through. Each cracked disk was also subjected to tensile energy that was reflected up the chain by the subsequent cracked disks in the assembly. This resulted in sufficiently high tensile loading of the first two cracked disks to cause crack growth as shown in the eleventh to twentieth frames in Figs 28 and 29. This was in contrast to the single 50% cracked disk experiment, for which crack growth was never observed. In certain multiple cracked disk experiments the tensile loading was high enough to cause multiple crack growth within the same disk, as shown in the nineteenth and twentieth frames in Fig. 28. The average crack velocities were determined to be 250 m s^{-1} for all these experiments.

As for the earlier experiments, two contacts preceding the cracked disks and two contacts following the cracked disks were analyzed using the photoelastic data. The corresponding contact load profiles for the two multiple cracked disks experiments are shown in Figs 30 and 31. The multiple cracked disks behave like filters. The aligned arrangement of cracks allowed greater energy to transfer across the cracked disks than the staggered arrangement. This resulted in a 40% peak contact load attenuation in the stress wave pulse locally as it propagated through the cracked disks for the staggered arrangement compared with only 30% for the aligned assembly. Also both the assemblies resulted in elongation of the loading pulse.

Strain gage experiments were also conducted for these two assemblies. The duration of the stress wave pulse increased from 120 to 210 μs for both cases, as the pulse propagated through the arrangement of cracked disks. Moreover, the overall attenuation, as determined from strain gage data, was 45% for both arrangements for 1 m of travel. This was only a slight increase over the 35% attenuation that was observed for a single 50% cracked disk assembly.

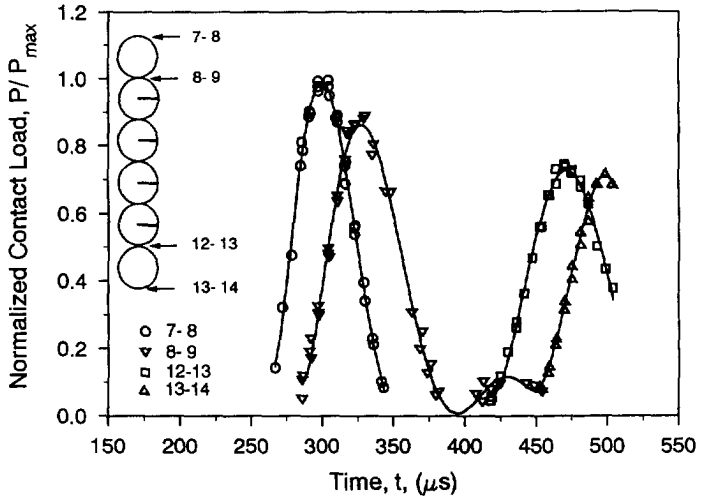

Fig. 30. Variation of normal contact loads as a function of time for a single chain assembly containing multiple cracked disks with aligned cracks.

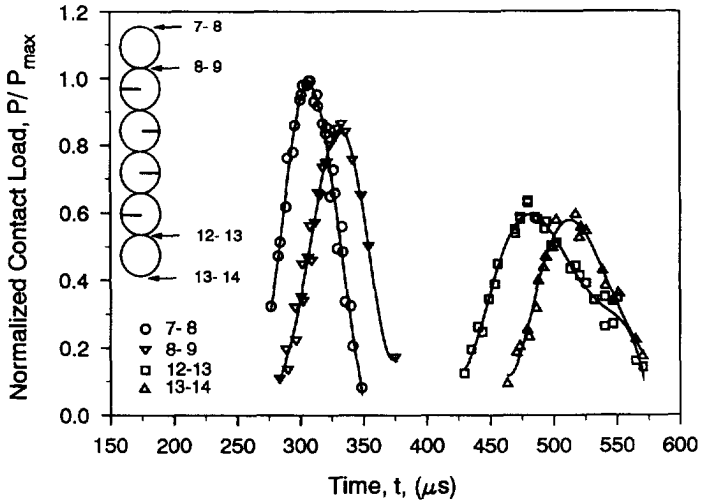

Fig. 31. Variation of normal contact loads as a function of time for a single chain assembly containing multiple cracked disks with staggered cracks.

5. SUMMARY

The presence of damaged particles influences stress wave propagation through a granular medium. The effects of varying crack length and crack orientation on the transmitted stress wave pulse are summarized as follows.

(1) The stress field in the cracked particle was a superposition of the contact and the crack tip stresses. The crack tip was loaded in pure mode I or in combined mode I and mode II conditions depending on the orientation of the crack. However, the nature of the stresses in the undamaged particles adjacent to the cracked particles was not affected and Hertz stress field equations could still be used for stress analysis of these particles.

(2) As the length of the crack was increased from 0 to 75% of the disk diameter the average peak contact load attenuation also increased. This occurred due to the multiple reflections caused by the free surface of the crack. The presence of a crack also caused energy to be reflected back up the chain.

(3) In experiments with a single 75% pre-cracked disk considerable crack closure occurred resulting in substantial strain energy being stored in the cracked particle. This energy was subsequently released causing a large elongation in the stress wave pulse.

(4) As the orientation of the cracked particle was varied the load transfer characteristics changed. However, the far field peak contact load attenuation showed little dependence on the angle between the crack and the tangent plane of contact.

(5) All orientations of the cracks caused local elongation of the loading pulse. As the elongated pulse travelled, it decomposed into multiple wavelets. The secondary wavelets dissipated within a propagational distance of 1 m leaving a wave with a characteristic wavelength of four disk diameters.

(6) The average velocity of the stress wave pulse remained unaffected in these experiments.

(7) Certain crack orientations were found to be more conducive to crack initiation and growth. Crack growth occurs due to tensile loading of the crack tip from multiple reflections of the stress wave pulse within the pre-cracked disk. The tensile loading becomes dominant only towards the tail end of the incoming stress wave pulse, and that is when crack growth was observed. Crack growth results in dissipation of energy and rearrangement of the microstructural fabric of the particulate aggregate.

Acknowledgements—The support of the U.S. Air Force Office of Scientific Research under grant number FQ8671-93-00-936 is gratefully acknowledged.

REFERENCES

Brant, H. (1955). A study of the speed of sound in porous granular media. *J. Appl. Mech.* **22,** 479–486.
Duffy, J. and Mindlin, R. D. (1957). Stress–stain relation and vibration of a granular medium. *J. Appl. Mech.* **24,** 585–593.
Dvorkin, J., Mavko, G. and Nur, A. (1991). The effect of cementation on the elastic properties of granular material. *Mech. Mater.* **12,** 207–217.
Gassman, F. (1951). Elastic waves through a packing of spheres. *Geophysics* **16,** 673–685.
Hughes, D. S. and Cross, J. H. (1952). Elastic wave velocities in rocks at high pressures and temperature. *Geophysics* **17,** 577–593.
Iida, K. (1939). The velocity of elastic waves in sand. *Bull. Earthquake Research Inst., Japan,* **17,** 783–807.
Rossmanith, H. P, Editor (1983). *Rock Fracture Mechanics.* CISM Courses and Lectures, NO. 275. International Center of Mechanics and Science. Springer, Wien, New York.
Sadd, M. H., Tai, Q. M. and Shukla, A. (1993). Contact law effects on wave propagation in particulate materials using distinct element modelling. *Int. J. Nonlinear Mech.* **28,** 251–265.
Shin, J. G. and Karr, D. G. (1990). Propagation of continuum damage in a nonlinear viscoelastic bar by finite difference method. *AMD* Vol. 109, *ASME,* 237–249.
Shukla, A. and Nigam, H. (1985). A numerical–experimental analysis of the contact stress problem. *J. Strain Anal.* **20,** 241–245.
Shukla, A., Sadd, M. H., Xu, Y. and Tai, Q. M. (1993). Influence of load pulse duration on dynamic load transfer in a simulated granular medium. *J. Mech. Phys. Solids* **41,** 1795–1808.
Smith, J. O. and Liu, C. K. (1953). Stresses due to tangential and normal loads on an elastic solid with application to some contact problems. *J. Appl. Mech.* **20,** 157–166.
Takahashi, T. and Sato, Y. (1949). On the theory of elastic waves in granular substance. *Bull. Earthquake Research Inst., Japan* **27,** 11–16.
Thornton, C. and Barnes, D. J. (1986). Computer simulated deformation of compact granular assemblies. *Acta Mech.* **64,** 45–61.
Ting, J. M. and Corkum, B. T. (1992). A computational laboratory for discrete element geomechanics. *J. Comput. Civil Engng, Am. Soc. Civil Engrs* **6,** 129–146.
Zhu, C. Y., Shukla, A. and Sadd, M. H. (1991). Prediction of dynamic contact loads in granular assemblies. *J. Appl. Mech.* **58,** 341–346.